Geochemistry Geophysics Geosystems G3

Article
Volume 11, Number 10
8 October 2010
Q10004, doi:10.1029/2010GC003178
ISSN: 1525-2027

Published by AGU and the Geochemical Society

Mass spectrometric ^{3}He measurement in ^{4}He-rich phases: Techniques and limitations for cosmogenic ^{3}He dating of zircon, apatite, and titanite

William H. Amidon and Kenneth A. Farley

Geological and Planetary Sciences Division, California Institute of Technology, 1200 East California Boulevard, Pasadena, California 91125, USA (wamidon@gps.caltech.edu)

[1] Recent calibration studies have expanded the range of target minerals suitable for cosmogenic ^{3}He dating to include U and Th-rich phases such as zircon, apatite, and titanite. These minerals often contain large amounts of radiogenic ^{4}He that present several analytical challenges for precise and accurate ^{3}He determinations. In this paper we document the abundance sensitivity and changes in the absolute sensitivity and time evolution of the ^{3}He signal over a wide range of ^{4}He pressures in a MAP 215-50 noble gas mass spectrometer. Large (>50%) decreases in sensitivity with ^{4}He amount arising from space charge effects were observed but can be corrected for using an isotope dilution–like technique in which ^{3}He spike is added to a sample midway through the mass spectrometric analysis. Large amounts of ^{4}He also cause the time evolution of the ^{3}He signal to become steeper, degrading precision of the initial peak height determination from the intercept. Taken together we find that these effects preclude reliable analysis of samples with ^{4}He > 1 μmol and that ^{3}He/^{4}He ratios of greater than ~5×10^{-10} are required to routinely measure ^{3}He to better than 20% precision. We present some general considerations by which to assess the probability of success of measuring cosmogenic ^{3}He in these phases as a function of elevation, exposure age, and helium cooling age.

Components: 5700 words, 6 figures, 1 table.

Keywords: helium; MAP 215-50; abundance sensitivity; noble gas; sensitivity.

Index Terms: 1105 Geochronology: Quaternary geochronology; 1150 Geochronology: Cosmogenic-nuclide exposure dating (4918); 1094 Geochemistry: Instruments and techniques.

Received 14 April 2010; **Revised** 20 July 2010; **Accepted** 29 July 2010; **Published** 8 October 2010.

Amidon, W. H., and K. A. Farley (2010), Mass spectrometric ^{3}He measurement in ^{4}He-rich phases: Techniques and limitations for cosmogenic ^{3}He dating of zircon, apatite, and titanite, *Geochem. Geophys. Geosyst.*, *11*, Q10004, doi:10.1029/2010GC003178.

1. Introduction

[2] Cosmogenic dating is a widely used tool for establishing exposure histories of both terrestrial and extraterrestrial surfaces. Because of its nuclear stability, high production rate from most target elements, and relative ease of measurement, ^{3}He is a particularly attractive nuclide for these studies. Efforts have been made to develop a diverse family of minerals amenable to cosmogenic ^{3}He dating; for example, cosmogenic ^{3}He production rates in apatite, zircon and titanite were recently determined [*Amidon et al.*, 2008, 2009; *Farley et al.*, 2006]. These particular minerals are ubiquitous on Earth and are therefore appealing dating targets, but they present a unique analytical challenge because they

often carry extremely high ^{4}He concentrations from U and Th decay. For several reasons such high concentrations can reduce the accuracy and precision of ^{3}He measurements. In this paper we document how high ^{4}He abundances degrade mass spectrometric ^{3}He measurements and present approaches by which to minimize these negative consequences. Ultimately the utility of these mineral phases for cosmogenic ^{3}He dating will hinge on the long-term geological history of the sample. Most notably, samples with old (U/Th)-He ages may not be suitable for cosmogenic ^{3}He dating due to excessively high ^{4}He contents. Based on these considerations we present constraints on the range of geological settings in which cosmogenic ^{3}He dating of apatite, zircon and titanite is likely to be successful.

[3] The presence of spallation produced cosmogenic ^{3}He in terrestrial samples was first recognized by researchers who had been focusing on measuring the trapped magmatic He component in olivine and pyroxene [*Craig and Poreda*, 1986; *Kurz*, 1986; *Lal*, 1987]. As a result, early applications of cosmogenic ^{3}He dating focused on olivine and pyroxene, and only recently has attention extended to more diverse mineral phases such as zircon, apatite, titanite, garnet, and Fe-Ti oxides [*Amidon et al.*, 2008; *Farley et al.*, 2006; *Gayer et al.*, 2004; *Kober et al.*, 2005; *Margerison et al.*, 2005]. Of these, the production rates in zircon and apatite are the best calibrated (against both ^{10}Be and ^{14}C), giving production rates of ~ 103 and 133 at g^{-1} a^{-1}, respectively [*Amidon and Farley*, 2010]. However, most of these calibration studies were performed on samples with (U/Th)-He ages of <6 Ma, which accordingly have relatively low concentrations of radiogenic ^{4}He. As the technique is applied more widely, the range of (U/Th)-He ages (a proxy for radiogenic ^{4}He), and exposure ages (a proxy for ^{3}He) that combine to give routinely measurable ^{3}He/^{4}He ratios must be defined.

[4] To place constraints on the geologic conditions in which cosmogenic ^{3}He dating in zircon, apatite, and titanite is likely to succeed, we must first understand the analytical limitations associated with measurement of small amounts of ^{3}He in the presence of large amounts of ^{4}He. We thus investigate the performance of the Caltech MAP 215–50 noble gas mass spectrometer when operated under high ^{4}He pressures and discuss how these performance characteristics place a lower limit on the measurable ^{3}He/^{4}He ratio. The three analytical issues discussed in this paper are (1) instrument sensitivity at ^{4}He pressures well above, and ^{3}He/^{4}He ratios well below, what can be achieved by external standards; (2) the ^{3}He/^{4}He ratio at which tailing of ^{4}He onto the ^{3}He beam becomes measurable; and (3) the effects of large amounts of ^{4}He on the accuracy of the regression used to convert the time evolution of the ^{3}He beam into a ^{3}He abundance.

2. Helium Extraction and Mass Spectrometry

[5] Helium extraction is performed by thermal degassing in a double-walled resistance furnace or by Nd-YAG laser heating of sample loaded in a platinum packet. In the resistance furnace, samples are heated to 1500°C for 20 min following standard procedures [*Patterson and Farley*, 1998]. However, in many cases a variant of the laser method developed for (U/Th)-He dating is preferred because grains can be recovered after He outgassing for additional analyses or to demonstrate sample purity [*House et al.*, 2000]. For cosmogenic dating, large (6 × 3 mm) platinum tubes are used, which can typically accommodate up to 35 mg of zircon or 25 mg of apatite. Previously degassed capsules are loaded with sample and placed into wells in a copper planchet. To minimize thermal conduction to the copper, the capsules are placed on top of small lengths of tungsten wire. The capsules are heated to about 1200°C by rastering the laser beam across the surface of the capsule for ~30 min. Although the exact temperature achieved by each sample is not monitored, complete degassing is verified by reextraction steps at the same temperature. Blanks obtained by lasing empty packets are indistinguishable from procedural blanks (i.e., the same gas handling procedure without lasing), and are typically ~5×10^{-6} fmol of ^{3}He and ~ 3.3 fmol of ^{4}He. In no cases were analyses limited by background counts or "dark noise," which was monitored at mass 2.7 in ten cycles totaling 100 s during each analysis. No background counts were recorded during any of the analyses, placing an upper limit of 0.001 cps on this signal.

[6] Following extraction, the evolved gas is exposed to a hot SAES getter and expanded into a ~1.5 L expansion volume. A ~1% aliquot is then analyzed in a Pfeiffer Prisma quadrupole mass spectrometer to obtain a ^{4}He measurement [*Wolf et al.*, 1996]. The remainder of the He is cryogenically focused and released into a MAP 215-50 magnetic sector mass spectrometer. This instrument uses a Nier-type

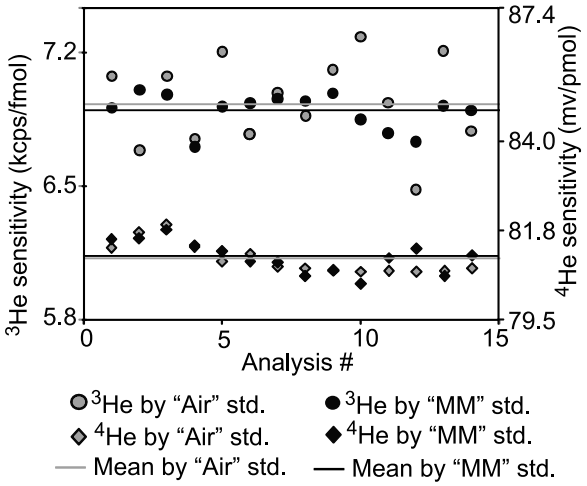

Figure 1. Results of 14 replicate standard analyses demonstrating that instrument sensitivity can be reliably determined by an isotope dilution approach. Shaded symbols denote instrument sensitivities determined by running the "Air" standard (^{3}He/^{4}He ratio of 2.05 Ra; ~4.4 pmol of ^{4}He) in the normal fashion. Solid symbols denote sensitivities determined by spiking the same "Air" standard with an aliquot of the "MM" standard (^{3}He/^{4}He ratio of 16.45 Ra; ~2.31 pmol of ^{4}He) midway through the analysis.

electron impact ion source, and measures the resulting ion signal by peak jumping between a Channeltron electron multiplier operated in pulse counting mode for ^{3}He and a Faraday cup with 10^{11} Ω resistor for ^{4}He. Most of the ~45 min sample collection time is devoted to counting ^{3}He ions using 30 s integrations and 600 s blocks. Measurements of the ^{4}He peak, as well as off-peak masses 2.7 and 3.2 are made for 30 s each between ^{3}He collection cycles.

[7] Simultaneous with this analysis, an aliquot of the "Murdering Mudpot" (MM) standard (16.45 Ra; ~2.31 pmol of ^{4}He) is prepared in the extraction line for use as an isotope dilution spike. The Murdering Mudpot standard was prepared from gas captured from a volcanic vent in Yellowstone National Park, Wyoming, U.S.A. After ~45 min of data acquisition on the sample this spike is introduced into the mass spectrometer. This results in a large increase in the ^{3}He signal without a significant change in the amount of ^{4}He or in sensitivity. This step allows the in-run ^{3}He sensitivity to be determined by fitting one regression line to the prespike ^{3}He data, and another to the postspike data. The linear fit applied to the prespike data is used to estimate the ^{3}He signal derived from the sample at time zero, and also to make a forward prediction of the signal generated by the sample at the time of the spike inlet. A second line is then fit to the postspike data, and is used to predict the combined signal from the sample and spike immediately after spike introduction. The difference between these two values is the net signal resulting from the ^{3}He in the spike, and is divided by the known amount of ^{3}He in the spike to estimate the ^{3}He sensitivity for each individual analysis.

[8] Calculation of the ^{3}He sensitivity (cps/pcc STP) by the spiking method is summarized by:

$$^3\text{He Sensitivity} = \left(B_{post} - \left(m_{pre} * T_{spike} + B_{pre\_spike}\right)\right) / \left[^3\text{He}_{std}\right] \quad (1)$$

where B_{post} denotes the beam intensity at the spike time (cps) extrapolated from a linear fit to the postspike data, m_{pre} denotes the slope of the prespike data (cps/s), T_{spike} denotes the spike time (seconds), and B_{pre_spike} denotes the intercept of the prespike data (cps), and $[^3\text{He}_{std}]$ denotes the amount of ^{3}He in the standard (pcc STP).

[9] Upon completion of the measurement, the mass spectrometer inlet valve is opened and the helium gas back-pumped to a turbomolecular pump. This step prevents exposure of the mass spectrometer ion pump to large amounts of ^{4}He, which we observed to become a source of ^{4}He following repeated exposure.

3. Determining Instrument Sensitivity

[10] The accuracy of the spiking technique was demonstrated by analyzing a series of 14 aliquots of the Caltech "Air" standard (^{3}He/^{4}He ratio of 2.05 Ra, ~4.4 pmol of ^{4}He) using this method. As shown in Figure 1, the sensitivity calculated from the mean of the 14 Air standards agrees to within 2% of the mean sensitivity computed from the 14 MM standard spikes. Likewise, the mean deviation between pairs of sensitivities computed by the Air and MM standards in a single analysis is ~2%. The ^{3}He sensitivities calculated from the 14 replicate MM spikes have a standard deviation of 1.3%, lower than the 3.5% for the replicate Air standards because the larger ^{3}He signal derived from the MM standard reduces the counting statistics error.

[11] It is necessary to spike our analyses because large amounts of ^{4}He result in space charge effects that lead to decreases in the sensitivity of the mass spectrometer. Figure 2 shows a compilation of ^{3}He sensitivities obtained for various amounts of ^{4}He under various tuning conditions over a several year

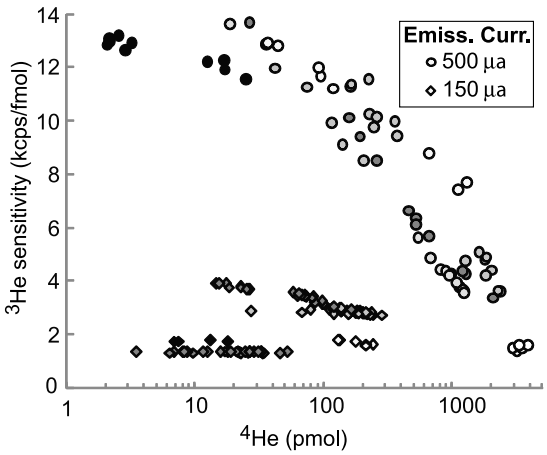

Figure 2. Instrument sensitivities determined during actual sample analyses at trap currents of either 500 μA (circles) or 150 μA (diamonds) for a variety of tuning conditions. Different tuning conditions are denoted by different shading. Note that the sensitivity decreases much more rapidly as function of ^{4}He pressure when running at 500 μA.

period that unambiguously document this effect. Although sensitivities up to ~13.5 kcps/fmol ^{3}He can be obtained by setting the trap current to 500 μa, the maximum ^{3}He sensitivity decreases rapidly with increasing ^{4}He amount. In contrast, when operated at a trap current of 150 μa, the sensitivity decreases much more slowly with increasing ^{4}He. It has been shown previously that the highest sensitivity is typically achieved near the ^{4}He pressure at which the mass spectrometer is tuned [*Burnard and Farley*, 2000]. Our data agree with this result, and it is thus possible that higher sensitivities can be obtained for high-^{4}He analyses at 500 μa by tuning the instrument at higher ^{4}He pressures.

4. Measurement of Low ^{3}He/^{4}He Ratios

[12] The feasibility of accurately measuring cosmogenic ^{3}He in high-^{4}He phases depends on the ^{3}He/^{4}He ratio of the mineral. For minerals with extremely low ^{3}He/^{4}He ratios ($<\sim10^{-9}$), generating a measurable ^{3}He signal often requires introduction of very large amounts of ^{4}He that may cause electrical arcing (electrical discharge through a gas) between the high-voltage plates of the ion source or cause measurable tailing of the ^{4}He peak (or the HD peak) onto the ^{3}He peak.

[13] The potential for arcing imposes a "technical" limit on the measurable ^{3}He/^{4}He ratio that can be estimated by combining estimates of the effective detection limit for ^{3}He with the ^{4}He pressure at which arcing is expected. Assuming a plate spacing of about 5 mm and a voltage difference of ~ 4 kV in the ion source, the Paschen equation [*Hartmann et al.*, 2000] indicates electrical discharge will occur at about 4 mbar He pressure. Given a volume of about 1 L in the MAP flight tube, this pressure corresponds to about ~0.2 μmol (~10^{17} atoms) of ^{4}He. Assuming a detection limit of 1 cps of ^{3}He and a sensitivity of 2.3 kcps/fmol ^{3}He (Figure 2), the absolute detection limit for ^{3}He at high ^{4}He pressure is ~3.7 fmol (~1×10^5 atoms). Combining these two values gives the lowest ^{3}He/^{4}He ratio at which ^{3}He can be accurately detected: about 1×10^{-12}. Attempts to measure ^{3}He in gas with a lower ^{3}He/^{4}He ratio would either yield a ^{3}He beam too small to accurately quantify, or amounts of ^{4}He so large that arcing would occur.

[14] Above this technical limit, the lowest measurable ^{3}He/^{4}He ratio is governed by the abundance sensitivity of the mass spectrometer as a function of the ^{4}He amount. In this discussion, we take abundance sensitivity to be defined as the fraction of ^{4}He atoms that fall on mass 3 during measurement of a pure ^{4}He beam. For example, an abundance sensitivity of 10^{-10} implies that if 10^{10} atoms of ^{4}He are introduced to the mass spectrometer, an average of one of those ^{4}He atoms falls on mass 3. Importantly, the abundance sensitivity is a function of the slit widths, which at Caltech and in other labs are commonly spaced to give a mass resolution (ΔM/M) of ~600 (relative to 10% peak height) for the MAP 215-50 instrument.

[15] To constrain this characteristic for the MAP 215-50, we used a sample of cosmic ray shielded thorianite (ThO_2) from Andalobe, Madagascar as a source of nearly pure ^{4}He. Thorianite was selected for its high ^{4}He production rate relative to other nuclear reactions (e.g., ^{6}Li(n, α)^{3}H) and because unlike ^{238}U, ^{232}Th does not undergo ternary fission, and therefore does not produce ^{3}He via fission. We established the ^{3}He/^{4}He ratio of the thorianite by running incrementally larger aliquots of He until a measurable ^{3}He signal was obtained. To ensure that no ^{4}He ions or HD ions were tailing onto mass 3 during these experiments, the ion count rate at mass 3.2 was monitored during the analysis and mass scans were performed immediately following the analysis (Figure 3). Because ^{3}He measurements were close to blank level the measured ^{3}He/^{4}He ratios have large errors. Nonetheless, four replicate analyses suggest the thorianite has a ^{3}He/^{4}He ratio of $0.54 \times 10^{-10} \pm 0.17 \times 10^{-10}$ (1σ) (Table 1). This value places on an upper

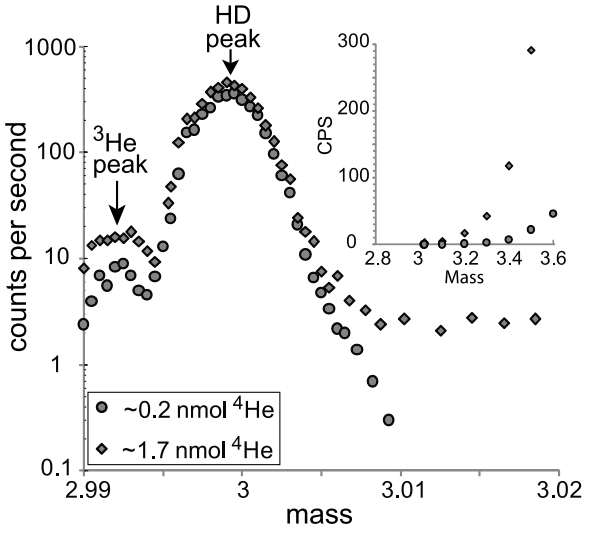

Figure 3. Mass scans performed on helium gas derived from a shielded thorianite sample. Samples with ~0.2 nmol of ^{4}He do not show tailing of ^{4}He ions onto mass 3, whereas samples with ~1.7 nmol of ^{4}He show significant tailing on this mass. The inset shows results of the same mass scans over a larger mass range, clearly demonstrating tailing of the ^{4}He peak.

limit on the abundance sensitivity of the MAP 215-50, which must be lower than ~0.54×10^{-10} at ^{4}He amounts near 0.5 nmol.

[16] Next, we analyzed successively larger aliquots of the thorianite-derived gas, monitoring mass 3.2 during each analysis to detect scattered ^{4}He ions. The presence of scattered ^{4}He ions at mass 3.2 was first detected at a ^{4}He amount of ~1.16 nmol (~7×10^{14} atoms). Mass scans up to 3.6 AMU demonstrate conclusively that the measured signal at mass 3.2 is due to tailing of the ^{4}He peak (Figure 3). Although the onset of detectable ^{4}He scattering appears abrupt, the limited number of experiments performed here are insufficient to determine whether the scattering results from self-similar growth of the ^{4}He peak, or from a change in the ^{4}He peak shape at higher pressures. Likewise, further experiments are required to determine how the threshold for severe ^{4}He tailing may change under different tuning conditions, although ~1.16 nmol (~7×10^{14} atoms) should provide a reasonable estimate for typical operating conditions.

5. Precision of ^{3}He Measurements

[17] A major factor controlling the precision of the ^{3}He concentration is the need to make a series of time-resolved ^{3}He measurements that document ion consumption and/or liberation of ^{3}He from surfaces within the mass spectrometer. These factors are usually eliminated by regressing the temporal evolution of the ^{3}He peak height to the time of inlet. The ^{3}He count rate typically decreases with time at very low ^{4}He amounts due to the consumption of ions. At high ^{4}He amounts, ^{3}He count rates typically increase with time due to scrubbing of ^{3}He atoms from the surfaces of the ionization chamber and detector by collisions with ^{4}He atoms. In almost all cases we find that ^{3}He count rate is a linear function of time justifying our use of linear regression techniques. Our experimental data show that the rise rate of the ^{3}He signal correlates with the amount of ^{4}He in the mass spectrometer (Figure 4).

[18] The uncertainty on the intercept of the ^{3}He evolution array increases as the slope of the line becomes steeper. Because the amount of ^{4}He exerts the strongest control on the slope of the array, the precision with which low ^{3}He signals can be determined depends on the amount of ^{4}He present. However, because the positive slope results from ^{3}He ions from previous samples implanted into the mass spectrometer (i.e., "memory"), this effect may

Table 1. Thorianite Measurements

	Mass 3 (amol)	1s	Mass 4 (nmol)	1s	^{3}He/^{4}He ($\times 10^{-10}$)	1s	Mass 3.2 (cps)
			No Detectable Tailing of ^{4}He Onto Mass 3				
TH1	0.010	0.002	0.22	0.01	0.47	0.11	0.0
TH2	0.015	0.004	0.22	0.01	0.72	0.22	0.0
TH3	0.023	0.006	0.36	0.01	0.64	0.14	0.0
TH4	0.013	0.005	0.41	0.01	0.33	0.10	0.0
Mean					0.54	0.10	
			Observed Tailing of ^{4}He Onto Mass 3				
TH5	0.530	0.036	1.49	0.04	3.55	0.43	0.5
TH6	1.700	0.072	4.50	0.13	3.78	0.41	5.0
TH7	1.898	0.081	4.98	0.15	3.81	0.41	5.0
TH8	4.219	0.180	11.19	0.34	3.77	0.41	20.0

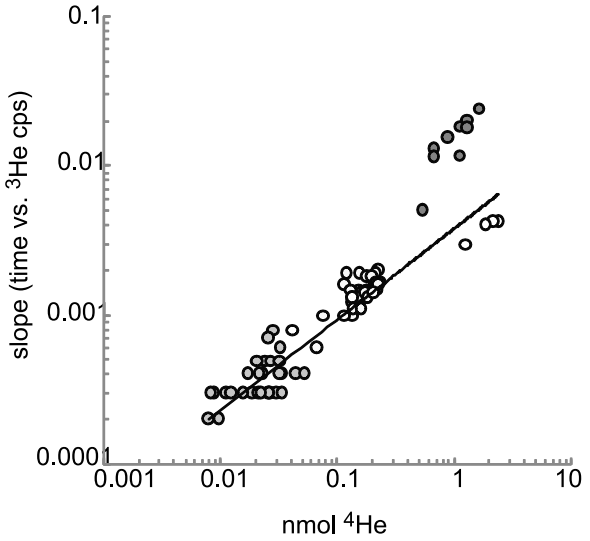

Figure 4. Slope of the time versus ^{3}He signal (counts per second) array for analyses run at a variety of ^{4}He pressures. Shading denotes analyses performed at different times and under different tuning conditions. The line reflects a linear fit to all of the data points except for the group of dark gray symbols with the highest slopes.

be lower in instruments with limited exposure to ^{3}He. This concept is evidenced by the two clusters of data points plotted at >0.5 nmol ^{4}He in Figure 4, which were collected at different times and plot on different trajectories due to different memory effects at the time of analysis. The total least squares regression line shown in Figure 4 is fit through all data points at <0.5 nmol ^{4}He and through only the "lower memory" cluster (unfilled symbols) at >0.5 nmol ^{4}He.

[19] To illustrate the approximate tradeoffs between slope and ^{3}He precision, we performed a Monte Carlo simulation in which a series of synthetic data sets (time versus ^{3}He counts) were produced for a range of ^{3}He signals from 0.5 to 3 cps. The first step was to determine the standard deviation of 18 actual data sets with negligible temporal evolution in ^{3}He. These standard deviations are plotted against ^{3}He beam size (cps) in Figure 5 and agree well with the standard deviations predicted from counting statistics. Synthetic data sets (time versus ^{3}He cps) with zero slope were then randomly created for 0.5, 1, 2, and 3 cps, each with a standard deviation predicted by counting statistics. Slopes of 0.001 to 0.01 (cps s^{-1}) were then applied to each synthetic data set and the uncertainty of the intercept determined for each slope. This process was repeated 500 times, and the mean uncertainty for each combination of signal intensity and slope was computed. The results (Figure 5) show that the error on the intercept is most sensitive to slope when the ^{3}He signal is <~1 cps.

6. Discussion

[20] The considerations described above define a minimum ^{3}He/^{4}He ratio above which ^{3}He in a sample can be reliably measured. The onset of severe tailing of the ^{4}He peak onto the ^{3}He peak occurs at ~1.16 nmol of ^{4}He (~7×10^{14} atoms), at which point the highest achievable ^{3}He sensitivity is near 2.3 kcps/fmol. At this sensitivity ~5.02 fmol (~135,000 atoms) of ^{3}He are required to generate a measurable signal of 0.5 cps, corresponding to a minimum measurable ^{3}He/^{4}He ratio of ~2×10^{-10}. Under typical operating conditions, a single analysis of a sample with a ^{3}He/^{4}He ratio of ~2×10^{-10} would be subject to an uncertainty of about 75%. However, because counting statistics scale as the square root of the counts, this uncertainty decreases rapidly as the ^{3}He/^{4}He ratio increases and the achievable ^{3}He cps rise above 0.5 cps.

[21] The lowest achievable uncertainty for a given ^{3}He/^{4}He ratio is determined by the ^{3}He count rate and the slope of the time versus ^{3}He array. As described above, these variables are determined by the sample size (i.e., the amount of ^{4}He released from the sample) and the instrument sensitivity. An inherent tradeoff exists when considering the

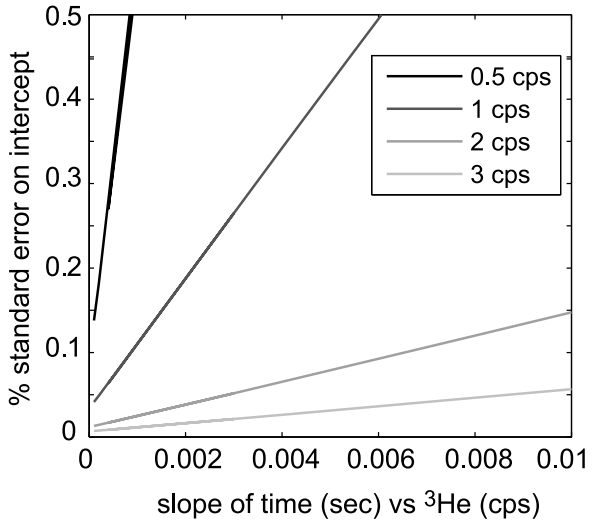

Figure 5. Results of the Monte Carlo calculations described in section 5. Samples with ^{3}He beam intensities of <1 count per second (cps) are particularly vulnerable to the increased errors imposed by steep slopes of the time versus ^{3}He cps array.

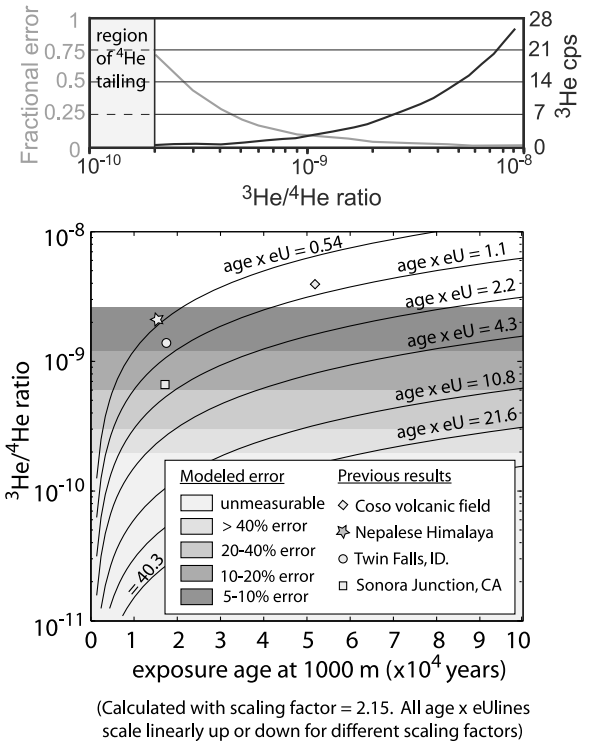

Figure 6. (top) The lowest analytical precision that can be achieved for a given ^{3}He/^{4}He ratio (black line) as determined by the Monte Carlo calculations described in section 5. The lowest precision is always achieved by running the largest possible sample size, corresponding to the plotted ^{3}He signal (gray line). (bottom) The evolution of ^{3}He/^{4}He ratios as a function of sample exposure age for a unique combination of (U-Th)/He closure age and effective U (eU) content. Note that the lines will shift up or down linearly for sample locations with higher or lower cosmogenic ^{3}He production rates, respectively. Shaded bands represent the approximate uncertainty with which ^{3}He can be determined on a single analysis of a sample with the given ^{3}He/^{4}He ratio assuming a relatively small "memory" effect as discussed in section 5.

sample size (i.e., ^{4}He signal) that yields the best precision for a given ^{3}He/^{4}He ratio. On the one hand, larger samples yield a larger ^{3}He signal that can be measured more precisely (Figure 5, top). However, this improved precision is offset by the loss of precision inflicted by the steeper slopes associated with high ^{4}He in larger samples (Figure 5, bottom). If it is assumed that sensitivity is roughly constant between ~0.9 and 1.16 nmol of ^{4}He (a reasonable approximation for the 150 μA conditions in Figure 2), a simple set of calculations can be made to determine the ideal sample size that should be run to yield the maximum precision.

[22] The calculations are performed by assuming a ^{3}He sensitivity of 2.3 kcps/fmol for all analyses. The slope of the ^{3}He versus time relationship for a given ^{4}He amount is taken from the fit to observed data shown by the line in Figure 4 and described above. The uncertainty as a function of slope and ^{3}He signal intensity is taken from the Monte Carlo calculations shown in Figure 5. For each ^{3}He/^{4}He ratio, an iterative search is then performed for the ^{4}He amount (a proxy for sample mass), that gives the lowest uncertainty for that ^{3}He/^{4}He ratio while also giving at least 0.5 cps of ^{3}He signal and less than 1.16 nmol of ^{4}He. Results in Figure 6 show that uncertainties of <20% (on a single analysis) can be routinely achieved for samples with ^{3}He/^{4}He ratios above ~5 × 10^{-10}. For all measurable ^{3}He/^{4}He ratios, the lowest error is always achieved by running the largest sample possible. In other words, the reduction in counting statistics error associated with running a larger sample always outweighs the added uncertainty introduced by steeper slopes of the ^{3}He versus time array. However, for any sample with a ^{3}He/^{4}He ratio >8 × 10^{-9} running the maximum sample size (i.e., approaching the threshold for ^{4}He tailing) yields a precision of less than 1%. Thus, as the ^{3}He/^{4}He ratio increases above a value of ~8 × 10^{-9}, proportionally smaller samples can be analyzed while still obtaining a 1% analytical precision. This calculation was repeated using a linear fit to the "high memory" points (filled symbols at >0.5 nmol ^{4}He) in Figure 4, and although errors were slightly higher in this case, the minimum error was still obtained by analyzing the largest sample possible in all cases.

[23] The minimum ^{3}He/^{4}He ratio that can be routinely measured (~2 × 10^{-10}) places fundamental limitations on the geological contexts within which cosmogenic ^{3}He dating is possible in apatite, titanite and zircon. Because ^{4}He is produced from radioactive decay of U and Th, the ^{4}He concentration in a mineral is a function of U and Th concentration and He closure age. The latter depends on both sample cooling history and on the mineral's He diffusivity. The closure temperatures of the accessory phases considered here are ~70°C for apatite and about ~180°C for both zircon and titanite. ^{3}He is produced via two distinct pathways: (1) cosmic ray neutron-induced spallation in the near surface and (2) low-energy neutron capture on ^{6}Li in both the near-surface and subsurface [*Amidon et al.*, 2008; *Farley et al.*, 2006]. For the purpose of this discussion, we will assume that production via Li can be ignored noting that the details of production from ^{6}Li have been discussed elsewhere [*Amidon et al.*, 2008; *Dunai et al.*, 2007;

Farley et al., 2006]. The amount of ^{3}He present in a sample is then a function of the local spallation production rate and the exposure age. For any given mineral, spallation production rates increase exponentially with increasing elevation and can decrease by as much as 50% from the poles to the equator [*Lal and Peters*, 1967]. As a consequence of these factors, high ^{3}He/^{4}He ratios are expected in samples with young He closure ages exposed at high elevations (e.g., a 100 ka ignimbrite erupted at 5000 m in Bolivia) for long time periods, whereas low ^{3}He/^{4}He ratios are expected from samples with old He closure ages exposed at lower elevations for shorter periods (e.g., a Holocene landslide deposit in coastal Australia).

[24] The trade-offs between exposure age and (U-Th)/He closure age on the precision of the ^{3}He determination are illustrated in Figure 6, which shows the expected ^{3}He/^{4}He ratio for apatite as a function of its cosmogenic exposure age, closure age and effective U (eU) content (defined as: [eU] = [U] + 0.235[Th]) [*Shuster et al.*, 2006]. Figure 6 allows the user to make a rough calculation of the expected ^{3}He/^{4}He ratio in minerals from a variety of geologic contexts. Each curved line represents the evolution of the ^{3}He/^{4}He ratio for a unique multiple of the closure age (Ga) and eU content (ppm). Overlain on the lines of constant eU*age are shaded bands that correspond to the approximate precision with which a single analysis of the given ^{3}He/^{4}He ratio can be performed. For comparison, we have plotted samples from the following geologic contexts: Tioga-aged (~18 ka) moraines from the Sierra Nevada (W. Amidon, unpublished data, 2009), metasedimentary rocks from moraines in the Nepal Himalaya [*Amidon et al.*, 2008], rhyolite surfaces from Coso, California [*Amidon et al.*, 2009] and Twin Falls, Idaho [*Amidon and Farley*, 2010]. It is important to note that the lines of constant eU*age in Figure 6 are generated using a sea level high-latitude production rate of 133 at g^{-1} a^{-1} and a scaling factor 2.15. For minerals with different production rates or different scaling factors, these lines will scale linearly up or down in ^{3}He/^{4}He space. Likewise, the analysis of multiple aliquots of the same sample can greatly improve the precision of the ^{3}He measurement for a given sample.

[25] Based on the above considerations, it is useful to consider which mineral phases are best suited for cosmogenic ^{3}He dating in different geologic contexts. For example, because apatite has a lower He closure temperature, lower eU content, and higher cosmogenic ^{3}He production rate, it often contains ^{3}He/^{4}He ratios that are 5–50 times higher than zircons from the same rock [*Amidon et al.*, 2008, 2009]. This means that apatite is the preferred mineral to work with in geological terranes with (U-Th)/He ages >~50 Ma. However, purifying large quantities of zircon or titanite is typically easier than purifying apatite because of their higher abundance and because strong acids can be used during purification. Large samples are a great benefit because more large unbroken grains are available, and because replicate samples can be run to improve the precision. Additionally, zircon tends to survive much better in fluvial and marine environments, making it an obvious choice for detrital studies.

7. Conclusions

[26] Recent calibration studies have shown that apatite, zircon and titanite are suitable phases for cosmogenic ^{3}He dating. However, the precision and accuracy with which ^{3}He can be measured in these phases may be limited by the potentially large amount of ^{4}He from the decay of U and Th over geologic time. Based on the characteristics of a typical MAP 215-50 noble gas mass spectrometer, we conclude that the lowest ^{3}He/^{4}He ratio that can be routinely measured is ~2×10^{-10}. Ratios higher than ~5×10^{-10} are required to achieve a precision of better than 20% on a single analysis. These constraints arise from the need to generate a ^{3}He signal of >~0.5 count per second, while not exceeding a threshold ^{4}He concentration of ~1.16 nmol of ^{4}He at which point tailing of the ^{4}He peak begins to compromise the ^{3}He measurement. While a broad range of (U-Th)/He closure ages and exposure histories will produce mineral phases with ^{3}He/^{4}He ratios >~5×10^{-10}, there are limitations to applications of cosmogenic ^{3}He dating in apatite, zircon, or titanite in geological terranes with (U-Th)/He closure ages >~50 Ma, exposure ages of <5 ka, or at sites very close to sea level.

Acknowledgments

[27] This manuscript benefited greatly from reviews by Rainer Wieler and two anonymous reviewers. This work was supported by NSF-EAR 0921295.

References

Amidon, W. H., and K. A. Farley (2010), Cosmogenic ^{3}He dating of apatite, zircon and pyroxene from Bonneville flood erosional surfaces, *Quat. Geochronol.* doi:10.1016/j.quageo.2010.03.005.

Amidon, W., et al. (2008), Anomalous cosmogenic ^{3}He production and elevation scaling in the high Himalaya, *Earth Planet. Sci. Lett.*, *265*, 287–301, doi:10.1016/j.epsl.2007.10.022.

Amidon, W. H., et al. (2009), Cosmogenic ^{3}He and ^{21}Ne production rates calibrated against ^{10}Be in minerals from the Coso volcanic field, *Earth Planet. Sci. Lett.*, *280*, 194–204, doi:10.1016/j.epsl.2009.01.031.

Burnard, P. G., and K. A. Farley (2000), Calibration of pressure-dependent sensitivity and discrimination in Nier-type noble gas ion sources, *Geochem. Geophys. Geosyst.*, *1*(7), 1022, doi:10.1029/2000GC000038.

Craig, H., and R. Poreda (1986), Cosmogenic ^{3}He in terrestrial rocks: The summit lavas of Maui, *Proc. Natl. Acad. Sci. U. S. A.*, *83*, 1970–1974, doi:10.1073/pnas.83.7.1970.

Dunai, T., et al. (2007), Production of ^{3}He in crustal rocks by cosmogenic thermal neutrons, *Earth Planet. Sci. Lett.*, *258*, 228–236, doi:10.1016/j.epsl.2007.03.031.

Farley, K. A., et al. (2006), Cosmogenic and nucleogenic ^{3}He in apatite, titanite, and zircon, *Earth Planet. Sci. Lett.*, *248*, 451–461, doi:10.1016/j.epsl.2006.06.008.

Gayer, E., et al. (2004), Cosmogenic ^{3}He in Himalayan garnets indicating an altitude dependence of the ^{3}He/^{10}Be production ratio, *Earth Planet. Sci. Lett.*, *229*, 91–104, doi:10.1016/j.epsl.2004.10.009.

Hartmann, P., et al. (2000), Effect of different elementary processes on the breakdown in low-pressure helium gas, *Plasma Sources Sci. Technol.*, *9*, 183–190, doi:10.1088/0963-0252/9/2/311.

House, M. A., et al. (2000), Helium chronometry of apatite and titanite using Nd-YAG laser heating, *Earth Planet. Sci. Lett.*, *183*, 365–368, doi:10.1016/S0012-821X(00)00286-7.

Kober, F., et al. (2005), In situ cosmogenic ^{10}Be and ^{21}Ne in sanidine and in situ cosmogenic ^{3}He in Fe-Ti-oxide minerals, *Earth Planet. Sci. Lett.*, *236*, 404–418, doi:10.1016/j.epsl.2005.05.020.

Kurz, M. D. (1986), Cosmogenic helium in a terrestrial igneous rock, *Nature*, *320*, 435–439, doi:10.1038/320435a0.

Lal, D. (1987), Production of ^{3}He in terrestrial rocks, *Chem. Geol.*, *66*, 89–98.

Lal, D., and B. Peters (1967), Cosmic ray produced radioactivity in the Earth, in *Handbuch der Physik*, vol. XLVI/2, edited by K. Geiss, pp. 551–612, Springer, Berlin.

Margerison, H. R., et al. (2005), Cosmogenic ^{3}He concentrations in ancient flood deposits from the Coombs Hills, northern Dry Valleys, East Antarctica: Interpreting exposure ages and erosion rates, *Earth Planet. Sci. Lett.*, *230*, 163–175, doi:10.1016/j.epsl.2004.11.007.

Patterson, D. B., and K. A. Farley (1998), Extraterrestrial ^{3}He in seafloor sediments: Evidence for correlated 100 kyr periodicity in the accretion rate of interplanetary dust, orbital parameters, and Quaternary climate, *Geochim. Cosmochim. Acta*, *62*, 3669–3682, doi:10.1016/S0016-7037(98)00263-4.

Shuster, D. L., et al. (2006), The influence of natural radiation damage on helium diffusion kinetics in apatite, *Earth Planet. Sci. Lett.*, *249*, 148–161, doi:10.1016/j.epsl.2006.07.028.

Wolf, R. A., et al. (1996), Helium diffusion and low-temperature thermochronometry of apatite, *Geochim. Cosmochim. Acta*, *60*, 4231–4240, doi:10.1016/S0016-7037(96)00192-5.